

Coulomb Branch of $\mathcal{N} = 4$, $d = 2 + 1$ Supersymmetric Gauge Field Theories

Sun Woo Kim
CID: 00939015

Supervisor: Professor Amihay Hanany
Assessor: Professor Daniel Waldram

19th February, 2018

Word Count: 5991

Submitted in partial fulfillment of the requirements for the degree of *Bachelor of Science*

Acknowledgements

I would like to thank Professor Amihay Hanany for giving me a chance to take a peek into the weird and wonderful world of symmetry, geometry, and field theories. I would not have had the chance to be exposed to such concepts had it not been for this project.

I would like to thank Santiago Cabrera for his passion and patience. He helped us wrap our head around the many difficult mathematical and physical concepts contained in this article. Without his explanations we would not have progressed as much as we did.

Special thanks goes to Rudolph Kalveks and Anton Zajac with equipping us with the computational tools required to proceed with the more daunting cases.

Finally, I would like to thank Jiashuo Zhang, Zhaozhen Tong, Alvaro L. Martinez, and my project partner for the insightful discussions which greatly helped with our understanding.

Abstract

Moduli space of a gauge field theory is an abstract space of vacuum expectation values of scalar fields. It is of physical significance as a point in this space must be chosen before the masses of particles can be determined. For $\mathcal{N} = 4, d = 2 + 1$ supersymmetric gauge field theories, whose information can be encoded in quiver diagrams, there are two branches in its moduli space: the Higgs branch and the Coulomb branch, where the latter can be calculated using the monopole formula. In this article, the Coulomb branch of A_n, C_n, F_4, G_2 Dynkin quivers and their affine counterparts were studied by calculating their Hilbert series using the monopole formula. In addition to confirming previous predictions, new implications on the choice of ungauging location (fixing one of the phases) were found, which we state as the *ungauging hypothesis*.

Summary

The project had two main components. The first was to understand the physical background and the mathematical ‘rules of the game’ behind quiver gauge theories. The second was calculate the Hilbert series, which encodes information the moduli space of a theory. The calculations were both analytic and computational.

The structure of the article is as follows. Sec. 1 introduces the reader to gauge field theories. It discusses the importance of symmetry, that the moduli space is an abstract space of vacua, and that it can be calculated using the Hilbert series via the monopole formula. Sec 2. covers the basic intuitions and mathematical concepts in representation theory, and the role of Hilbert series in algebraically describing spaces such as orbifolds. Sec. 3 and 4 deals with the specifics of the Coulomb branch of $\mathcal{N} = 4, d = 2 + 1$ quiver gauge theories, the problems in resolving the Hilbert series, and the methods employed to tackle them. Finally Sec. 5 and 6 discusses the findings some of which confirm the earlier claims and some which we believe to be new findings, which leads us to the *ungauging hypothesis*. We discuss further work to be done to test it.

The project, which took place in term 2, was evenly distributed between my project partner and I. However, I had partially worked on the project in term 1 while my partner did not. The work for the A_n quiver was completed during that time.

Contents

1	Introduction	6
2	Mathematical Background	7
2.1	Moduli Space	7
2.2	Groups and Representations	7
2.3	Root Systems and Dynkin Diagrams	9
2.4	Orbifolds	10
2.5	Hilbert Series	11
3	Quiver Gauge Theories	12
3.1	Background	12
3.2	Quiver Diagrams	12
3.3	QGT Monopole Formula	13
3.3.1	Summation Limits	13
3.3.2	Conformal Dimension	13
3.3.3	Topological Charge	14
3.3.4	Dressing Factor	14
3.4	Excess and Balance	15
3.5	Ungauging Scheme	16
3.6	Forms of Hilbert Series	17
4	Methods	18
4.1	Computation Methods	18
4.1.1	Shifting Sums	18
4.1.2	Counting Cases	18
4.1.3	Separation of Cases	19
4.2	Deducing Properties	19
5	Results and Discussion	19
5.1	Dynkin Quivers	19
5.1.1	A_n	20
5.1.2	C_n	21
5.1.3	F_4	21

5.1.4	G_2	21
5.1.5	Comments	22
5.2	Affine Dynkin Quivers	22
5.2.1	\hat{A}_n	22
5.2.2	\hat{C}_n	23
5.2.3	\hat{F}_4	24
5.2.4	\hat{G}_2	24
5.2.5	Comments	24
5.3	Ungauging Location	25
5.3.1	A_n, \hat{A}_n	25
5.3.2	C_n	25
5.3.3	F_4, G_2	26
5.3.4	\hat{F}_4, \hat{G}_2	27
5.3.5	Comments	27
6	Conclusion and Outlook	27

1 Introduction

Our best and most successful understanding of fundamental particles, the Standard Model, is a gauge field theory. *Field theory* meaning that the equation of motion, the Lagrangian, is governed by a set of scalar fields $\{\hat{\psi}_i(x)\}$ defined at every point in space-time, and *gauge theory* meaning that transforming the configurations of $\hat{\psi}_i(x)$'s in the Lagrangian by some symmetry group action leaves the Lagrangian invariant. For the Standard Model, this symmetry is famously described by the product of three symmetry groups, $U(1) \times SU(2) \times SU(3)$.

However, the Standard Model is incomplete; it cannot unify gravity with the other fundamental forces. This is one of the biggest unsolved problems in physics today. One attempt to unify the forces is via supersymmetry (SUSY), which adds a higher level of symmetry by linking fermions, the matter particles, with bosons, the force carriers.

In a gauge field theory, each scalar field has a *vacuum expectation value* $\langle \hat{\psi}_i \rangle$, or VEV for short. There also exists a scalar potential $\hat{\mathcal{W}}(\{\hat{\psi}_i\})$, a function of these scalar fields, where it is required that $\hat{\mathcal{W}} = 0$ for a vacuum. The configurations of VEVs, $\langle \hat{\psi}_i \rangle$'s where $\hat{\mathcal{W}} = 0$ can be described as an abstract space; this is called a *moduli space* [6]. A moduli space describes the space of vacua, and is the topic of interest for this article. They are important because a point in this space must be chosen before masses of particles can be determined. Moduli spaces, some of which are ‘folded’ spaces called *orbifolds*, can be algebraically described by functions called *Hilbert series* (HS). These will be discussed later.

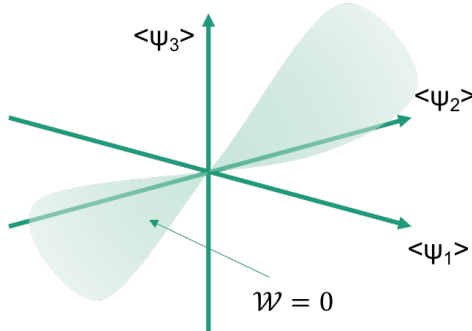


Figure 1: A diagram of a moduli space, embedded in a space of scalar field VEVs.

This article considers the Coulomb branch of $\mathcal{N} = 4$, $d = 2 + 1$ supersymmetric gauge field theories, where \mathcal{N} corresponds to ‘the number of supersymmetries’, $d = 2 + 1$ to 2 spatial and 1 temporal dimensions, and *Coulomb branch* refers to one part of the moduli space, the other being the ‘Higgs branch’. They are hereby referred to as *quiver gauge theories* (QGTs). It is a family of toy theories where the only parameters are the gauge symmetry groups, ones that can be encoded in diagrams called *quiver diagrams*. This family is considered to be the simplest of its kind, and is considered to be the building blocks to understand higher theories.

Recently, the *monopole formula* was proposed for QGTs [3], which simplified the computation of the HS of the Coulomb branch, allowing the construction of it from only the quiver diagram and a simple set of formulas. The main objective of this article is to study

the Coulomb branches and symmetries of various QGTs by calculating their respective Hilbert series, and to develop an intuition and understanding of the mathematics behind them.

2 Mathematical Background

2.1 Moduli Space

For $\mathcal{N} = 4$, $d = 2 + 1$ supersymmetric gauge field theories (QGTs), the moduli space has two branches: the Higgs branch and the Coulomb branch. To illustrate what a branch is, we examine a simple model.

Example. XYZ Model

One of the simplest example of a moduli space is the XYZ Model [2]. Turns out, a supersymmetric gauge theory in $4d$ can have a scalar potential $\hat{\mathcal{W}}$ described by three scalar fields, as:

$$\hat{\mathcal{W}}(\hat{\psi}_1, \hat{\psi}_2, \hat{\psi}_3) = |\hat{\psi}_1 \hat{\psi}_2|^2 + |\hat{\psi}_1 \hat{\psi}_3|^2 + |\hat{\psi}_2 \hat{\psi}_3|^2. \quad (2.1)$$

Recall that at a vacuum, $\hat{\mathcal{W}} = 0$. Then the three solutions, or the three branches of moduli space, are

$$\hat{\psi}_1 \neq 0; \hat{\psi}_2 = \hat{\psi}_3 = 0 \implies \langle \hat{\psi}_1 \rangle \in \mathbb{C}; \langle \hat{\psi}_2 \rangle = \langle \hat{\psi}_3 \rangle = 0, \quad (2.2a)$$

$$\hat{\psi}_2 \neq 0; \hat{\psi}_1 = \hat{\psi}_3 = 0 \implies \langle \hat{\psi}_2 \rangle \in \mathbb{C}; \langle \hat{\psi}_1 \rangle = \langle \hat{\psi}_3 \rangle = 0, \quad (2.2b)$$

$$\hat{\psi}_3 \neq 0; \hat{\psi}_1 = \hat{\psi}_2 = 0 \implies \langle \hat{\psi}_3 \rangle \in \mathbb{C}; \langle \hat{\psi}_1 \rangle = \langle \hat{\psi}_2 \rangle = 0. \quad (2.2c)$$

For each branch, the free VEV can have any complex value; therefore each branch is the space of \mathbb{C} . Note that the three branches are equal at the origin when all values are equal to zero. Turns out, this point is physically important because this is where ‘extra massless states’ arise.

Just as the XYZ displays branches in its moduli space, the moduli space of $\mathcal{N} = 4$, $d = 2 + 1$ supersymmetric gauge field theories has the Higgs branch and the Coulomb branch, which agree at the origin. The Higgs branch is simple to calculate but the Coulomb branch is infamously difficult due to quantum corrections it receives. In the cases dealt in this article, the space of Coulomb branch are *orbifolds* and *varieties*; discussed later.

2.2 Groups and Representations

To understand the necessary concepts and the results, we introduce basic intuitions of group and representation theory.

Consider a set of transformations $\{g_i\}$ all of which keeps some object, say the equation of motion, invariant. Also suppose that applying one transformation, g_a , after another, g_b , corresponds to another single transformation, g_c . Denoting this as a multiplication, $g_c = g_a \cdot g_b$. This structure can be abstractly encoded in a mathematical object called a group. For continuous transformations, there is a continua of group elements. Turns out,

there is a class of continuous groups called compact Lie groups, where each group element can be thought of as a point on a manifold, with a ‘multiplication’ defined.

Groups can also be ‘represented’ as transformations in vector spaces, as *representations*:

Definition. Representation

A representation ρ of a group \mathcal{G} is map between each group element $g \in \mathcal{G}$ and matrix $\rho(g)$ such that group structure is preserved. That is, if $g_a \cdot g_b = g_c$, then $\rho(g_a) \cdot \rho(g_b) = \rho(g_c)$.

Clearly, the representations are matrices in vector spaces, so one example of ‘group action’ is multiplication by representations on a set of vectors. Turns out, representations of compact Lie groups are indexed by a tuple of non-negative integers called *highest weights*. The compact Lie groups dealt in this article, labeled with Alphabets, or by their alternate names, are

$$A_n = SU(n + 1), B_n = SO(2n + 1), C_n = Sp(n), D_n = SO(2n), E_{6,7,8}, \text{ and } F_4,$$

where the number n in the subscript corresponds to the number of parameters in the highest weights.

Definition. Character of a Representation

Character $\chi_{[\text{highest weights}]}^{\mathcal{G}}$ of representation of group \mathcal{G} is the trace of representation ρ parameterised by the highest weights.

Example. $A_1 = SU(2)$

Elements of the continuous group $SU(2)$ is parameterised by rotation angle θ . Its representations are parameterised by highest weight l' . Its character is

$$\chi_{[l']}^{SU(2)}(\theta) = e^{-il'\theta} + e^{-i(l'-2)\theta} + \dots + e^{-il'\theta} \quad (2.3)$$

The character can be written in different basis. In $y = e^{i\theta}$ basis,

$$\chi_{[l']}^{SU(2)}(y) = y^{-l'} + y^{-(l'-2)} + \dots + y^{l'} \quad (2.4)$$

As an aside, we note that defining $s = l'/2$, and $x = e^{i\theta/2}$, s corresponds to angular momentum number and the exponent of each term to angular momentum projection number m , from quantum mechanics:

$$\chi_{[l']}^{SU(2)}(x) = x^{-l} + x^{-(l-1)} + \dots + x^l. \quad (2.5)$$

We can also note that the character can be thought of as a points on a lattice. For the example of $SU(2)$, we can think of y as a vector called a *weight vector* and its exponents as its components. Then each term in the character is a point in \mathbb{R} , as shown in Fig. 2.



Figure 2: The weight lattice of $SU(2)$.

We can see that the character forms a lattice of points; we call it the *weight lattice*. In general, the weight lattice lives in \mathbb{R}^n space where n is the number of parameters in highest weights.

2.3 Root Systems and Dynkin Diagrams

In the most general sense, root systems are a system of vectors. It can be represented with a Dynkin diagram, where each node denotes a root vector α_i , and each edge, which can be weighted-directed, denotes the relationship between two root vectors. The relations are summarised in Fig. 3. Dynkin diagrams relevant to the article are shown in Fig. 4.












α_i	Edge	α_j	$\theta_{i,j}$	$\frac{ \alpha_i ^2}{ \alpha_j ^2}$
			90°	1
			120°	1
			135°	2
			150°	3

Figure 3: A table of Dynkin diagram rules. Any two disconnected nodes make 90° to each other

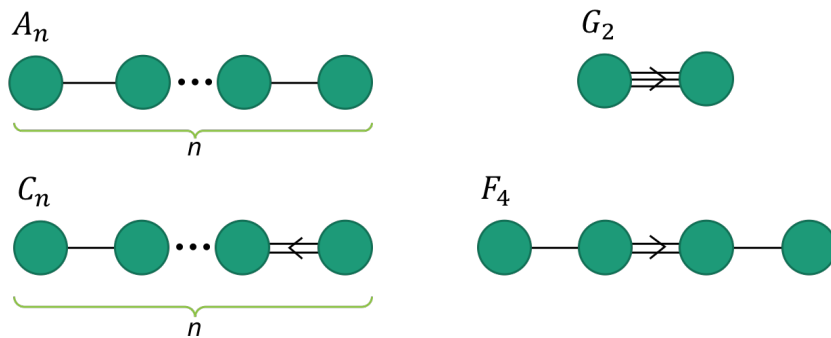


Figure 4: Relevant Dynkin diagrams; each represent a root system

Example. C_2

Consider the Dynkin diagram C_2 . This produces two vectors, α_1, α_2 where $2\alpha_1^2 = \alpha_2^2$ and $\theta_{1,2} = 135^\circ$. Then, the root system can be constructed as Fig. 5.

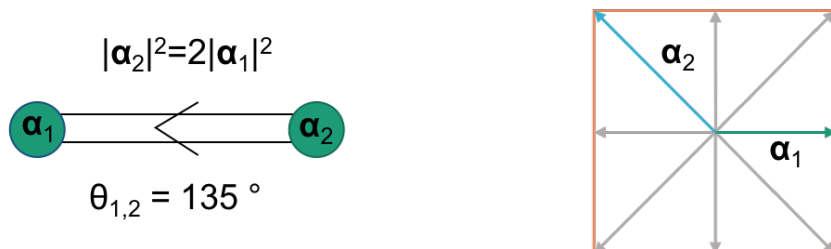


Figure 5: The Dynkin diagram for C_2 (left) and the resulting root system (right)

Dynkin diagrams and Lie groups (of the same name) are related in the following sense: the root vectors $\{\alpha_i\}$ (of Dynkin diagrams) can be directly related to the fundamental weight vectors $\{y_i\}$ (from characters) using a *Cartan matrix* that can be constructed from the Dynkin diagrams. Also, the vector from any one weight to another in the weight lattice can be written as a sum of root vectors with integer components.

A Cartan matrix \mathbf{C}_{st} (where s denotes source, t denotes target, denoting node index), is constructed with 2's on the diagonal, 0 if unconnected, and $-\lambda$ if connected, where weighting $\lambda = 1$ unless for a directed-weighted edge, if $s \rightarrow t$ follows the 'arrow', then λ is the weighting of the edge.

Example. G_2

For G_2 (shown as one of the examples in Fig. 4), the transformation from weight basis to root basis is

$$\begin{pmatrix} \alpha_1 \\ \alpha_2 \end{pmatrix} = \begin{pmatrix} 2 & -3 \\ -1 & 2 \end{pmatrix} \begin{pmatrix} y_1 \\ y_2 \end{pmatrix} \quad (2.6)$$

where $\mathbf{C}_{12} = -3$, since the edge between α_1 and α_2 is weighted-directed by weighting 3, and $1 \rightarrow 2$ follows the 'arrow'.

2.4 Orbifolds

An orbifold \mathcal{M}/\mathcal{G} is a manifold \mathcal{M} acted upon by a finite group \mathcal{G} , where \mathcal{G} 'marries' different points in \mathcal{M} together, 'folding' it in to an orbifold. For a more precise definition, an *orbit* must be defined.

Definition. Orbit

An orbit $\mathcal{O}(p \in \mathcal{M}; \mathcal{G})$ of a point $p \in \mathcal{M}$ by group \mathcal{G} is the set of points that p goes to under each group element $g_i \in \mathcal{G}$.

Example. $\mathcal{O}(p \in \mathbb{C}^2; \mathbb{Z}_2)$

Let $p = (p_1, p_2)^T$ be a vector in \mathbb{C}^2 . The two group elements g_1, g_2 of \mathbb{Z}_2 can be written as matrix representations $\rho(g_i)$ in \mathbb{C}^2 , as

$$\rho(g_1) = \begin{pmatrix} 1 & 0 \\ 0 & 1 \end{pmatrix}; \quad \rho(g_2) = \begin{pmatrix} -1 & 0 \\ 0 & -1 \end{pmatrix}. \quad (2.7)$$

In this case, group action by element g_i is given by $\rho(g_i) \cdot p$, so

$$\mathcal{O}(p \in \mathbb{C}^2; \mathbb{Z}_2) = \{\rho(g_1) \cdot p, \rho(g_2) \cdot p\} = \{p, -p\}. \quad (2.8)$$

Definition. Orbifold.

An orbifold, \mathcal{M}/\mathcal{G} of manifold \mathcal{M} and finite group \mathcal{G} is space of all orbits:

$$\frac{\mathcal{M}}{\mathcal{G}} = \{\mathcal{O}(p; \mathcal{G}) \mid p \in \mathcal{M}\} \quad (2.9)$$

Definition. Singularity.

A singularity of an orbifold is a point in which group action leaves the point invariant.

Example. $\mathbb{C}^2/\mathbb{Z}_2$

So $\mathbb{C}^2/\mathbb{Z}_2$ can be seen as all the coordinates married with their negatives, i.e.

$$\frac{\mathbb{C}^2}{\mathbb{Z}_2} = \{\{p, -p\} \mid p \in \mathbb{C}^2\}. \quad (2.10)$$

Note that the point $p = (0, 0)^T$ is a singularity, since $p = -p = (0, 0)^T$.

2.5 Hilbert Series

Orbifolds can also be described algebraically, using a Hilbert series (HS).

Definition. Hilbert Series

A refined Hilbert series of fugacity t , $H(t)$, is a function that when series expanded about $t = 0$, the term of each order of t enumerates every unique monomial of that order.

So, in case of an orbifold of \mathcal{M}/\mathcal{G} , the HS enumerates every unique monomial of \mathcal{M} that is invariant under \mathcal{G} .

Example. \mathbb{C}^2

One of the simplest example of a Hilbert series is the flat space of \mathbb{C}^2 . Using two variables x and y for each dimension, we see that the unique monomial of order 0 is $1 = x^0y^0$, of order 1 are x, y , of order 2 are x^2, xy, y^2 and so on. The refined Hilbert series that encodes this is

$$H_{\mathbb{C}^2}(x, y, t) = \frac{1}{(1 - xt)(1 - yt)} = 1 + (x + y)t + (x^2 + xy + y^2)t^2 + \dots \quad (2.11)$$

we can ‘unrefine’ the Hilbert series by setting $x = y = 1$. Then the series only counts the number of monomials:

$$H_{\mathbb{C}^2}(t) = \frac{1}{(1 - t)^2} = 1 + 2t + 3t^2 + \dots \quad (2.12)$$

Example. $\mathbb{C}^2/\mathbb{Z}_2$

Now let’s consider a \mathbb{Z}_2 action on \mathbb{C}^2 . Since we are looking for monomials that are invariant under the transformation $(x, y) \rightarrow (-x, -y)$, we can easily see that all the monomials of odd powers are not invariant. Then the Hilbert Series can be written as

$$\begin{aligned} H_{\mathbb{C}^2/\mathbb{Z}_2}(x, y, t) &= \frac{1}{2} \left(\frac{1}{(1 + xt)(1 + yt)} + \frac{1}{(1 - xt)(1 - yt)} \right) \\ &= 1 + (x^2 + xy + y^2)t^2 + \dots \end{aligned} \quad (2.13)$$

We can also define $X := x^2, Y := y^2, Z := xy$, as variables to describe $\mathbb{C}^2/\mathbb{Z}_2$ algebraically. These variables are called *generators* as they can be multiplied generate all the \mathbb{Z}_2 invariant monomials. Since the three generators are related as $XY = Z^2$, the equation of a cone, $\mathbb{C}^2/\mathbb{Z}_2$ is homeomorphic to ‘complex cone’, embedded in \mathbb{C}^3 . From this, we can see that \mathbb{Z}_2 action also created curvature on an originally flat \mathbb{C}^2 space.

3 Quiver Gauge Theories

3.1 Background

In a supersymmetric gauge field theory, each scalar field (bosons) has a superpartner [12]. The theory is invariant under rearrangement between the two by some symmetry group; these interchange operators are called *supercharges*. There also exists another symmetry called R-symmetry, where the configurations of supercharges themselves can be rearranged with a symmetry group without affecting the physics.

Collection of scalar fields with their SUSY partners are called *multiplets*, or *superfields*. For QGTs, there are two types of multiplets: *vectormultiplets* and *hypermultiplets*. On the Coulomb branch, VEVs of scalar fields of vectormultiplets are non-zero, whereas on the Higgs branch, VEVs of scalar fields of hypermultiplets are non-zero. Turns out, because vectormultiplets contain gauge couplings, the Coulomb branch receives quantum corrections in low-energy scales. This made it difficult to calculate.

For the Coulomb branch, the total symmetry always contains with R-symmetry with another factor. This extra factor is hereby referred to as ‘global symmetry’ [6], and one of the main features of the theories.

3.2 Quiver Diagrams

QGTs can be described pictorially using a quiver diagram. A quiver diagram, with an example shown in Fig. 6, is a weighted-directed graph composed of nodes and edges. It encodes information about a QGT. From only this diagram and the *monopole formula* which will be discussed later, the expression for the Hilbert series for Coulomb branch the moduli space can be constructed.

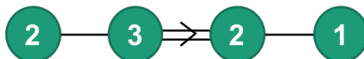


Figure 6: An example of a quiver; this one looks like the F_4 Dynkin diagram.

On a quiver, each node corresponds to a vectormultiplet, corresponding to a local gauge group, (bosons). For this article, only *unitary quivers*, whose nodes are of unitary groups were studied. The number N inside each node represents the rank of the unitary gauge group $U(N)$. Each node with rank N_i holds N_i ‘GNO/monopole charges’, which are of interest in the construction of the HS.

Each edge corresponds to a hypermultiplet, corresponding to a matter particle (fermion). It connected to a node if it is charged under the node’s gauge group. An edge can be weighted-directed, in which case it is represented by an ‘inequality’ and doubling/tripling of the lines; this is shown on the edge between the $U(3)$ and $U(2)$ node in the example in Fig. 6. The monopole charges on the bigger side of the ‘inequality’ are scaled by the number of lines. If a quiver has no weighted-directed edges, it is said to be *simply laced*.

3.3 QGT Monopole Formula

Recently, the monopole formula, which greatly simplifies the calculation of the Coulomb branch, was introduced [3]. It is in Eq. (3.1):

$$H(\mathbf{z}, t) = \sum_{\{\mathbf{m}_i\}} \left(t^{2\Delta(\{\mathbf{m}_i\})} \prod_{i=1}^{\#\text{nodes}} z_i^{J(\mathbf{m}_i)} P_i(\mathbf{m}_i, t) \right) \quad (3.1)$$

where

$\#\text{nodes}$ is the number of nodes in the quiver,

\mathbf{z} denotes $(z_1, \dots, z_{\#\text{nodes}})$, the topological fugacities of each node,

t denotes the fugacity,

$\{\mathbf{m}_i\}$ denotes the set of monopole charges, with the i^{th} node contributing $\mathbf{m}_i = \{m_{i,1}, \dots, m_{i,N_i}\}$ charges, and N_i is the rank of the $U(N_i)$ node,

Δ is the conformal dimension,

$J(\mathbf{m}_i)$ is the topological charge,

and finally $P_i(\mathbf{m}_i, t)$ is the classical dressing factor, which is itself piecewise with respect to relationships between a node's monopole charges, $\mathbf{m}_i = (m_{i,1}, \dots, m_{i,N_i})$.

This is the starting point for all calculations of Hilbert series of Coulomb branches. Although the derivation of the monopole formula is non-trivial, the interpretation is as follows: the Hilbert series for the Coulomb branch counts gauge invariant ‘monopole operators’ (which themselves are parameterised by GNO charges, $\{\mathbf{m}_i\}$), over all possible charge configurations [10]. This describes the Coulomb branch because there exists a one-to-one correspondence between gauge invariant dressed monopole operators (the physical operators) and the holomorphic polynomials that form the holomorphic ring (that mathematically describes the space) of the Coulomb branch [3, 8]. Each factor will be discussed in detail.

3.3.1 Summation Limits

Each node i contributes $\mathbf{m}_i = (m_{i,1}, \dots, m_{i,N_i})$ monopole charges, where a charge can be an integer. For unitary quivers, the summand is summed over all possible configurations of monopole charges, with the limits $(\infty > m_{i,1} \geq \dots \geq m_{i,N_i} > -\infty)$ for each node. That is, for each node, the summation operator is

$$\sum_{m_{i,1}=m_{i,2}}^{\infty} \sum_{m_{i,2}=m_{i,3}}^{\infty} \dots \sum_{m_{i,N_i-1}=m_{i,N_i}}^{\infty} \sum_{m_{i,N_i}=-\infty}^{\infty} . \quad (3.2)$$

3.3.2 Conformal Dimension

For the cases of unitary quivers, conformal dimension is given by

$$2\Delta = \sum_{nodes} 2\Delta_{node} + \sum_{edges} 2\Delta_{edge} \quad (3.3)$$

where for node i it is the sum of all the possible differences between its charges:

$$2\Delta_{node} = -2 \sum_{j>k}^{N_i} |m_{i,j} - m_{i,k}|, \quad (3.4)$$

and for each edge connected to node i and i' , it is all the possible differences of charges between the two nodes:

$$2\Delta_{edge} = \sum_{j=1}^{N_i} \sum_{k=1}^{N_{i'}} |\lambda_i m_{i,j} - \lambda_{i'} m_{i',k}| \quad (3.5)$$

where the weighting $\lambda_i = 1$ except for the case of weighted-directed edge where the charges of node on the bigger side of the ‘inequality’ has λ_i equal to the weight of the edge. Physically, the conformal dimension Δ for a given configuration of GNO charges corresponds to the energy of this state [9].

A quiver is *good* if for all possible values of $\{\mathbf{m}_i\}$, $2\Delta > 1$, *ugly* if there exists some cases where $2\Delta = 1$ such that $2\Delta \geq 1$, and *bad* if there exists any values such that $2\Delta < 1$ [4]. This article only deals with good and ugly quivers; the monopole formula only works for good and ugly quivers.

The form of the conformal dimension is what makes resolving the Hilbert series computationally challenging, as all cases of inequalities must be considered. Once all the different cases are considered, the series is simply a product and sum of infinite geometric series.

3.3.3 Topological Charge

For each node carrying a $U(N)$ gauge symmetry, noting the Bianchi identity on its field strength suggests that there is an additional ‘conserved current’, $J^{(1)}$ [11]. Since there is a conserved quantity, Noether’s theorem suggests there exists an additional global $U(1)_J$ symmetry. This is called the topological, or hidden symmetry. It is said to be hidden because none of the basic fields are charged under it; however, it happens that monopole operators do interact with this symmetry and carry ‘topological charges’. We keep track of these via topological fugacities, \mathbf{z} The topological charge for node i , $J(\mathbf{m}_i)$, is given by

$$J(\mathbf{m}_i) = \sum_{j=1}^{N_i} m_{i,j} \quad (3.6)$$

3.3.4 Dressing Factor

For a given node i holding $\mathbf{m}_i = (m_1, \dots, m_{N_i})$ monopole charges, its dressing factor is constructed using the partition of the monopole charges of the node, $\boldsymbol{\lambda}(\mathbf{m}_i) = (\lambda_1(\mathbf{m}_i), \lambda_2(\mathbf{m}_i), \dots)$. A partition can be constructed from a Young’s tableau, where the rule to construct one is as below.

1. From a list of numbers $\mathbf{a} = (a_1, \dots, a_N)$, on the first row, from left to right, draw as many boxes as the frequency of the smallest number on the list \mathbf{a} .
2. For $n = 2$ to N , on the n^{th} row, from left to right, draw as many boxes as the frequency of the n^{th} smallest number on the list \mathbf{a} .
3. Then, λ_k is equal to the number of boxes on the k^{th} column; $k = 1, 2, 3, \dots$

Then, the dressing factor for node i given by

$$P_i(\mathbf{m}_i, t) = \prod_{j=1}^{\#columns} \frac{1}{(1 - t^{2j})^{\lambda_j(\mathbf{m}_i)}}. \quad (3.7)$$

Example. $U(2)$ Node

Consider a node with rank $N = 2$. Then its monopole charges are (m_1, m_2) . Given the limits of the sums, there are two cases: $m_1 = m_2$, and $m_1 > m_2$. The Young tableau for both cases are shown in Fig. 7

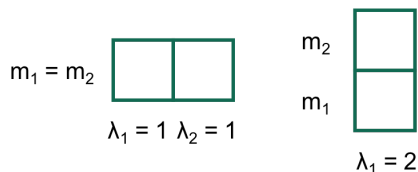


Figure 7: Two constructions of Young's tableau, for $m_1 = m_2$ (left) and $m_2 > m_1$ (right).

Considering the two cases, the dressing factor for this node can be written as

$$P(\mathbf{m}, t) = \begin{cases} \frac{1}{(1-t^2)^2} & m_1 > m_2 \\ \frac{1}{(1-t^2)(1-t^4)} & m_1 = m_2 \end{cases}. \quad (3.8)$$

So, the dressing factor is a piecewise function.

It happens that when GNO charges are not equal, the gauge group are broken into smaller, residual gauge groups; for the example, when $m_2 > m_1$, the $U(2)$ gauge group is broken into $U(1) \times U(1)$. Essentially, the dressing factor ‘dresses’ the monopole operators to make sure they include other scalar fields from the vectormultiplet that are invariant under the new residual gauge group, so that the HS includes all and only the invariant monopole operators.

3.4 Excess and Balance

For each node, a notion of *excess* can be established, where for node i , its excess ϵ_i is

$$\epsilon_i = (\text{weighted sum of neighbour's ranks}) - 2 \cdot (\text{own rank}), \quad (3.9)$$

where a neighbouring node is weighed by 1 unless the neighbour is connected by a weighted-directed edge, and is on the smaller side of the ‘inequality’. If so, its rank is weighed by the weighting of the edge.

Fig .8 shows that the example quiver has three nodes balanced and one minimally imbalanced. For the $U(3)$ node, the weighted ranks of neighbours ranks are 2 from the left and 2 from the right (as it is on the smaller side of the ‘inequality’), so $\epsilon = (2+2 \times 2) - (2 \times 3) = 0$.

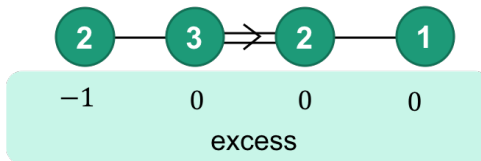


Figure 8

A node is said to be *balanced* if $\epsilon_i = 0$, *minimally imbalanced* if $\epsilon_i = -1$, and *imbalanced* otherwise.

A quiver is good if all nodes have $\epsilon_i \geq 0$, and can be ugly if there are some minimally imbalanced nodes and bad if any of the nodes have $\epsilon_i < -1$.

3.5 Ungauging Scheme

The monopole formula reveals that the HS sums over all possible differences of GNO charges. Since the sum is over infinities, and the conformal dimension has terms of absolute value of difference of charges, without any constraints, there are infinite terms for each order of t ; the HS diverges.

We can constrain one of the charges by ‘ungauging’ a node, which is a mathematical trick where ungauging the i^{th} node alters the HS as

$$\sum_{m_{i,1}} \rightarrow 1, \tag{3.10a}$$

$$P_i(t) \rightarrow P_i(t) \cdot (1 - t^2), \text{ and} \tag{3.10b}$$

$$m_{i,1} \rightarrow 0, \tag{3.10c}$$

setting one of the monopole charges to zero [10]. On the quiver diagram, if the node was of $U(1)$, it becomes a square with a ‘1’ inside of it. If it was of $U(N_i > 1)$, it becomes a ‘squircle’, with the same N_i written inside of it. The two cases are differentiated as the former case’s HS is equivalent to switching the node to a flavour node of $SU(1)$ (not discussed in this article) and holds no charge, but the latter case is only a mathematical trick and still holds $N_i - 1$ charges. Fig. 9 illustrates the Quiver shown in Fig. 6 ungauged at different locations.

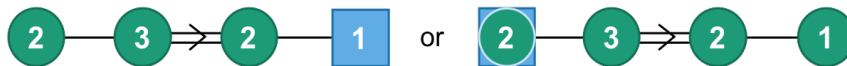


Figure 9: The example quiver with a $U(1)$ node ungauged (left) and a $U(2)$ node ungauged (right).

Since $U(1)$ transformation refers to a shift in phase $e^{i\theta}$, ungauging is setting one of the phases to zero, factoring out the $U(1)$ of a $U(N)$ node. For a good or ugly quiver, once a node is ungauged, the Hilbert Series is sufficiently constraint to converge.

The notion of ‘long’ and ‘short’ nodes can also be defined. Long nodes are nodes on the greater side of the ‘inequality’, or all nodes of a simply laced quiver. Short nodes are nodes on the smaller side of the ‘inequality’. This is shown in Fig. 10.



Figure 10: Long and short nodes

3.6 Forms of Hilbert Series

In order to extract information about the global symmetry and the moduli space, the Hilbert series is resolved into a more convenient form.

Similarly to Sec. 2.5, an *unrefined* Hilbert series is where all the topological fugacities are set to 1, ($z_i \rightarrow 1$), and the *refined* HS is the original HS with topological charges as is.

Because a HS in principle can be broken down into geometric sums, it is possible to write it in a rational form. From the unrefined form of the rational form it is possible to deduce the moduli space for simple cases as Sec. 2.5.

In some cases, it is also possible to write the Hilbert series as series expansions of t , where each term is a character of a representation of a group with the highest weights that is a function of orders of t .

It turns out that the t^2 term corresponds to the character of the *adjoint representation* of the gauge symmetry group in terms of the topological fugacities, \mathbf{z} , where the adjoint representation is defined as representation whose character’s dimension is same as the group’s. Therefore from the t^2 term of the series, the global symmetry group can be deduced.

Sec. 2.2 showed that characters can have multiple basis. Therefore, in general, a *fugacity map* from the quiver’s basis to a more familiar weight basis $\{y_i\}$ may be necessary.

Consider a quiver’s basis $\mathbf{z} = (z_1, \dots, z_{\#})$ and weight basis $\mathbf{y} = (y_1, \dots, y_{\#})$. The fugacity map from \mathbf{z} to \mathbf{y} can be represented in matrix form with an operator (*):

$$\begin{pmatrix} z_1 \\ \vdots \\ z_{\#} \end{pmatrix} = \begin{pmatrix} a_{11} & \cdots & a_{1\#} \\ \vdots & \ddots & \vdots \\ a_{\#1} & \cdots & a_{\#\#} \end{pmatrix} * \begin{pmatrix} y_1 \\ \vdots \\ y_{\#} \end{pmatrix} \quad (3.11)$$

which denotes that $z_j = \prod_{k=1}^{\#} y_k^{a_{jk}}$, such that each element of the ‘vector’ is raised to power by the matrix element and multiplied over instead. For a transformation between root and weight basis, the Cartan matrix would be the transformation matrix.

Plethystic exponential, $\text{PE}[f(x_1, \dots, x_n)]$, of a function $f(x_1, \dots, x_n)$ is defined to be [5]

$$\text{PE}[f(x_1, \dots, x_n)] = \exp \left(\sum_{k=0}^{\infty} \left[\frac{f(x_1^k, \dots, x_n^k)}{k} \right] \right). \quad (3.12)$$

It can be used to write long HSs compactly. For example, it can be shown that

$$\text{PE}[(z_1 + z_1^{-1} + z_2 + z_2^{-1})t] = \frac{1}{(1 - z_1 t)(1 - z_1^{-1} t)(1 - z_2 t)(1 - z_2^{-1} t)} \quad (3.13)$$

by using the identity that $\ln(1 - x) = \sum_{k=0}^{\infty} \frac{x^k}{k}$.

4 Methods

4.1 Computation Methods

In general resolving the HS using the monopole formulas is a tedious task. The three methods used are outlined in the following sections.

4.1.1 Shifting Sums

For rank 1 nodes, the limits of the sums are $(-\infty, \infty)$. Therefore shifting the indices by any finite amount keeps the limits the same. Take the case of the HS of the quiver A_2 (Fig. 11)

$$\frac{1}{(1 - t^2)^2} \sum_{m_1=-\infty}^{\infty} \sum_{m_2=-\infty}^{\infty} z_1^{m_1} z_2^{m_2} t^{|m_1 - m_2| + |m_2|}. \quad (4.1)$$

shifting $m_1 \rightarrow m_1 + m_2$,

$$= \frac{1}{(1 - t^2)^2} \left(\sum_{m'_1=-\infty}^{\infty} z_1^{m'_1} t^{|m'_1|} \right) \left(\sum_{m_2=-\infty}^{\infty} (z_1 z_2)^{m_2} t^{|m_2|} \right) \quad (4.2)$$

Now the two summations are separated into simple geometric sums which can be found to be

$$\begin{aligned} &= \frac{1}{(1 - t^2)^2} \left(\frac{1 - t^2}{(1 - z_1 t)(1 - z_1^{-1} t)} \right) \left(\frac{1 - t^2}{(1 - z_1 z_2 t)(1 - z_1^{-1} z_2^{-1} t)} \right) \\ &= \frac{1}{(1 - z_1 t)(1 - z_1^{-1} t)(1 - z_1 z_2 t)(1 - z_1^{-1} z_2^{-1} t)} \end{aligned} \quad (4.3)$$

However, this method only worked for simple cases; for higher ranks, some limits are bounded by finite values. This meant that the coupling cannot be removed via shifting the sums.

4.1.2 Counting Cases

The second method was to explicitly count the number of cases for an order of t . Take the example of a general \hat{A}_n quiver, shown in Fig. 15. Shifting the sums, the conformal dimension can be found to be of the form

$$2\Delta = \left| \sum_{i=1}^n m_i \right| + \sum_{i=1}^n |m_i| \quad (4.4)$$

to find the global symmetry, for example, we are interested in the cases where $2\Delta = 2$. Note that for this condition, it is required that $\sum_{i=1}^n |m_i| \leq 2$. This means that there can be only two non-zeros of $m_i = \pm 1$, with the rest being 0. The possible configurations are

$$\begin{aligned}
2n \text{ cases : } & (\pm 1, 0, \dots, 0), (0, \pm 1, 0, \dots, 0), \dots, (0, \dots, 0, \pm 1) \\
n(n-1) \text{ cases : } & \left\{ \begin{array}{l} (+1, -1, 0, \dots, 0), (+1, 0, -1, \dots, 0, 0), \dots, (+1, 0, \dots, 0, -1) \\ (-1, +1, 0, \dots, 0), (0, +1, -1, \dots, 0, 0), \dots, (0, +1, \dots, 0, -1) \\ \vdots \\ (-1, 0, \dots, 0, +1), (0, -1, 0, \dots, 0, +1), \dots, (0, \dots, 0, -1, +1), \end{array} \right. \quad (4.5)
\end{aligned}$$

a total of $2n + n(n-1)$ cases. The dressing factor's t^2 term is n . Combining the all the contributions, we find that t^2 term is $2n + n(n-1) + n = (n+1)^2 - 1$ which corresponds to the dimension of group $A_n = SU(n+1)$ hence the global symmetry of the same group.

4.1.3 Separation of Cases

The third method was to separate out the cases. For example,

$$2\Delta = |m_1 - m_2| + |m_2 - m_3| = \begin{cases} m_1 - m_3 & \text{for } m_1 \geq m_2 \geq m_3 \\ -m_1 + 2m_2 - m_3 & \text{for } m_2 \geq m_1 \geq m_3 \\ m_1 - 2m_2 + m_3 & \text{for } m_1 \geq m_3 \geq m_2 \\ -m_1 + m_3 & \text{for } m_3 \geq m_2 \geq m_1 \end{cases} \quad (4.6)$$

After sorting the different cases, each sum is a geometric series. Accounting for all the dressing factors, the Hilbert series was calculated by summing over node by node. This was done computationally using RJK Weyl Utilities code, written in Mathematica by R. Kalveks. This method proved to be the most applicable, as many quivers were of high complexity, with many different inequalities to consider.

4.2 Deducing Properties

In general, the characters of each term are not in a familiar weight basis. Therefore, it can be tricky to recognise the characters and therefore the global symmetry of the HS. The first step was to unrefine the Hilbert series in order to find the dimension of the t^2 term. Its dimension would limit the possible global symmetry groups. Also from the unrefined rational form, the Coulomb branch could be determined in simple cases such as $\mathbb{C}^n/\mathbb{Z}_2$.

5 Results and Discussion

5.1 Dynkin Quivers

Below we present the results for *Dynkin quivers*, which are quivers that have the same structure as the Dynkin diagrams of the same names. Attempting to balance all nodes results in one or two minimally imbalanced nodes; we ungauged the quivers at one of the minimally imbalanced nodes.

5.1.1 A_n

The quiver corresponding to the Dynkin diagram A_n , shown in Fig. 11 is ungauged at the n^{th} node. To highlight the techniques, its calculation will be shown in more detail than other examples.

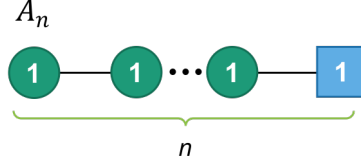


Figure 11

The Hilbert series, using the monopole formula, is

$$H_{A_n}(\mathbf{z}, t) = \frac{1}{(1-t^2)^{n-1}} \sum_{\{\mathbf{m}\}=-\infty}^{\infty} z_1^{m_1} z_2^{m_2} \dots z_{n-1}^{m_{n-1}} t^{2\Delta}, \quad (5.1)$$

where $\{\mathbf{m}\} = m_1, m_2, \dots, m_{n-1}$, and

$$2\Delta = |m_1 - m_2| + \dots + |m_{n-2} - m_{n-1}| + |m_{n-1}|. \quad (5.2)$$

Shifting the sum as $m_1 \rightarrow m_1 + m_2$, then $m_2 \rightarrow m_2 + m_3$, then ..., then $m_{n-2} \rightarrow m_{n-2} + m_{n-1}$, we see that the summations become independent of each other. Then the simple geometric series can be calculated and the Hilbert series can be written as

$$H_{A_n}(\mathbf{z}, t) = \text{PE} \left[\left(z_1 + z_1 z_2 + z_1 z_2 z_3 + \dots + \prod_{i=1}^{n-2} z_i + \prod_{i=1}^{n-1} z_i + \text{c.c.} \right) t \right] \quad (5.3)$$

where c.c. denotes complex conjugate of all the terms inside the bracket.

Via a fugacity map to weight basis \mathbf{y} ,

$$\begin{pmatrix} z_1 \\ z_2 \\ \vdots \\ z_{n-2} \\ z_{n-1} \end{pmatrix} = \begin{pmatrix} 1 & 0 & \dots & 0 & 0 \\ 2 & 1 & \dots & 0 & 0 \\ \vdots & \vdots & \ddots & \vdots & \vdots \\ (n-2) & (n-3) & \dots & 1 & 0 \\ (n-1) & (n-2) & \dots & 2 & 1 \end{pmatrix} * \begin{pmatrix} y_1 \\ y_2 \\ \vdots \\ y_{n-2} \\ y_{n-1} \end{pmatrix}, \quad (5.4)$$

we find that each term is a character of $Sp(n-1)$, and

$$H_{A_n}(\mathbf{z}, t) = \sum_{k=0}^{\infty} \chi_{[k,0,\dots,0]}^{Sp(n-1)}(\mathbf{z}) t^k, \quad (5.5)$$

displaying a $Sp(n-1)$ global symmetry. By unrefining the series, it is clear from Eq. (5.3) that

$$H_{A_n, \text{unref}}(t) = \frac{1}{(1-t)^{2(n-1)}} = H(\mathbb{C}^{2(n-1)}), \quad (5.6)$$

a flat space.

5.1.2 C_n

The C_n quiver is minimally imbalanced at the first node, and is shown in Fig. 12.

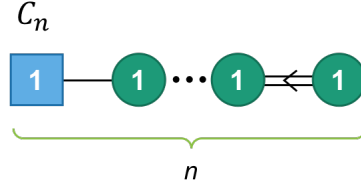


Figure 12

Explicitly computing the Hilbert Series for C_3, C_4, C_5 , we predict

$$H_{C_n}(\mathbf{z}, t) = \sum_{k=0}^{\infty} \chi_{[2k, 0, \dots, 0]}^{Sp(n-1)}(\mathbf{z}) t^{2k}, \quad (5.7)$$

again, displaying $Sp(n-1)$ global symmetry. From the unrefined series, it was found that

$$H_{C_n, unref}(t) = \frac{1}{2} \left(\frac{1}{(1+t)^{2(n-1)}} + \frac{1}{(1-t)^{2(n-1)}} \right) = H(\mathbb{C}^{2(n-1)}/\mathbb{Z}_2). \quad (5.8)$$

5.1.3 F_4

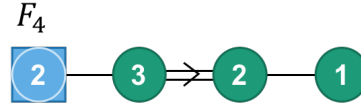


Figure 13

The F_4 quiver is minimally imbalanced on the leftmost node, as shown in Fig. 13. Explicitly solving, we find

$$H_{F_4}(\mathbf{z}, t) = \sum_{k=0}^{\infty} \chi_{[k, 0, 0, 0, 0, 0, 0]}^{Sp(7)}(\mathbf{z}) t^k, \quad (5.9)$$

$$H_{F_4, unref}(t) = H(\mathbb{C}^{14}), \quad (5.10)$$

which again demonstrates symplectic $Sp(7)$ global symmetry, and a flat Coulomb branch.

5.1.4 G_2

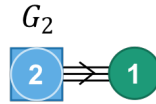


Figure 14

The G_2 quiver (Fig. 14) was solved with the results below:

$$H_{G_2}(\mathbf{z}, t) = \sum_{k=0}^{\infty} \chi_{[k, 0]}^{Sp(2)}(\mathbf{z}) t^k, \quad (5.11)$$

$$H_{G_2, unref}(t) = H(\mathbb{C}^4), \quad (5.12)$$

displaying a symplectic $Sp(2)$ global symmetry, and a flat Coulomb branch.

5.1.5 Comments

From all the results, found analytically (for A_n) and by explicit computations (for C_n, F_4, G_2), we find that the global symmetries are symplectic, with a flat Coulomb branch, except for the case of C_n , which displayed $\mathbb{C}^{2(n-1)}/\mathbb{Z}_2$ orbifolds. Note that for all nodes ungauged on long nodes are flat spaces but C_n , ungauged at a short node, has a \mathbb{Z}_2 action on the $\mathbb{C}^{2(n-1)}$ space.

5.2 Affine Dynkin Quivers

An *affine Dynkin quiver* connects a new node to the minimally imbalanced nodes of the dynkin quiver to make all nodes balanced. It is conventionally ungauged at the newly added node, and is notated with a hat ($\hat{}$) on top of the normal labeling.

5.2.1 \hat{A}_n

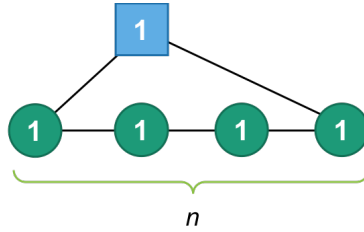


Figure 15

The HS of the quiver, \hat{A}_n (shown in Fig 15), given by the monopole formula, is

$$H_{\hat{A}_n}(\mathbf{z}, t) = \frac{1}{(1-t^2)^n} \sum_{\{\mathbf{m}\}=-\infty}^{\infty} z_1^{m_1} z_2^{m_2} \dots z_n^{m_n} t^{2\Delta}, \quad (5.13)$$

where $\{\mathbf{m}\} = m_1, m_2, \dots, m_n$, and

$$2\Delta = |m_1| + |m_1 - m_2| + \dots + |m_{n-1} - m_n| + |m_n|. \quad (5.14)$$

Shifting the sums as $m_1 \rightarrow m_1 + m_2$, then $m_2 \rightarrow m_2 + m_3$, then ..., then $m_{n-1} \rightarrow m_{n-1} + m_n$, we find that the form of the conformal dimension is as the case shown in Sec. 4.1.2, which shows that the global symmetry is $A_n = SU(n+1)$.

As for the general HS, from the first few cases it is clear that

$$H_{\hat{A}_n}(\mathbf{z}, t) = \sum_{k=0}^{\infty} \chi_{[k,0,\dots,0,k]}^{A_n}(\mathbf{z}) t^{2k}, \quad (5.15)$$

agreeing with the analytic prediction of the global symmetry. The HS corresponds to

$$H_{\hat{A}_n}(t) = H(\overline{\min}_{A_n}) \quad (5.16)$$

where $\overline{\min}_{A_n}$ denotes ‘the closure of the minimal nilpotent orbit of A_n ’. Closures of nilpotent orbits of compact Lie groups are another kind of space called *varieties*, different from manifolds and orbifolds. They are in general rich in structure.

5.2.2 \hat{C}_n

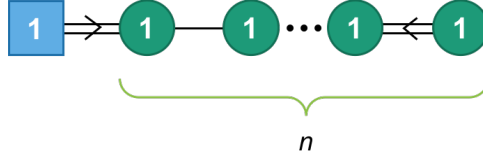


Figure 16

Note that the quivers $C_{n+1} = \hat{C}_n$ if ungauged at leftmost node; this is because a square (flavour) node contributes no charges, so the doubly-weighted arrow does not alter the HS. The complete HS, same as $H_{C_{n+1}}$, is

$$H_{\hat{C}_n, unref}(t) = H(\mathbb{C}^{2n}/\mathbb{Z}_2) = H(\overline{min}_{C_n}). \quad (5.17)$$

The global symmetry can be found analytically. consider the HS given by the monopole formula:

$$H_{\hat{C}_n}(\mathbf{z}, t) = \frac{1}{(1-t^2)^n} \sum_{\{\mathbf{m}\}=-\infty}^{\infty} z_1^{m_1} z_2^{m_2} \dots z_n^{m_n} t^{2\Delta}, \quad (5.18)$$

where $\{\mathbf{m}\} = m_1, m_2, \dots, m_n$, and

$$2\Delta = |m_1| + |m_1 - m_2| + \dots + |m_{n-2} - m_{n-1}| + |m_{n-1} - 2m_n|. \quad (5.19)$$

Shifting as $m_2 \rightarrow m_2 + m_1$, then $m_3 \rightarrow m_3 + m_2 + m_1$, then ..., then $m_{n-1} \rightarrow \sum_{i=1}^{n-1} m_i$, we find that the conformal dimension becomes

$$2\Delta = \left| 2m_n - \sum_{i=1}^{n-1} m_i \right| + \sum_{i=1}^{n-1} |m_i|. \quad (5.20)$$

To find the global symmetry, we seek the solutions for $2\Delta = 2$. Then it is required that $\sum_{i=1}^{n-1} |m_i| \leq 2$ as before. This means that there can be only two non-zeros of $m_{i \leq n-1} = \pm 1$, with the rest being 0, while m_n can be $-1, 0, +1$. We consider the case where $n \geq 3$.

For $m_n = 0$, the conformal dimension (Eq. (5.20)) is as same as one for \hat{A}_{n-1} ; therefore there are $2(n-1) + (n-1)(n-2) = n(n-1)$ cases.

For $m_n = +1$, the conformal dimension is

$$2\Delta = \left| 2 - \sum_{i=1}^{n-1} m_i \right| + \sum_{i=1}^{n-1} |m_i|. \quad (5.21)$$

which there are, for $n-1$ entries,

$$\begin{aligned} \binom{n-1}{2} \text{ cases : } & (1, 1, \dots, 0), (1, 0, 1, \dots, 0), \dots, (0, \dots, 1, 1) \\ (n-1) \text{ cases : } & (1, 0, \dots, 0), (0, 1, 0, \dots, 0), \dots, (0, \dots, 0, 1) \\ (n-1) \text{ cases : } & (2, 0, \dots, 0), (0, 2, 0, \dots, 0), \dots, (0, \dots, 0, 2) \\ 1 \text{ case : } & (0, 0, \dots, 0) \end{aligned} \quad (5.22)$$

Summing to $n(n+1)/2$ cases.

For $m_n = -1$, there are same number of cases as $m_n = +1$.

So, in total, the contribution from the conformal dimensions is $n(n-1) + 2 \times n(n+1)/2$. Combining with the n contribution from the dressing factor, the unrefined t^2 term is $n(2n+1)$, the dimension of the group $C_n = Sp(n)$, corresponding to the global symmetry of C_n . This agrees with the predicted series.

5.2.3 \hat{F}_4



Figure 17

The quiver for \hat{F}_4 is shown in Fig. 17. The HS was computed explicitly, and was found to be

$$H_{\hat{F}_4}(\mathbf{z}, t) = \sum_{k=0}^{\infty} \chi_{[k,0,0,0]}^{F_4}(\mathbf{z}) t^{2k}, \quad (5.23)$$

displaying an F_4 global symmetry. The Coulomb branch is:

$$H_{\hat{F}_4, unref}(t) = H(\overline{min}_{F_4}), \quad (5.24)$$

again not a flat space.

5.2.4 \hat{G}_2



Figure 18

The quiver for \hat{G}_2 is shown in Fig. 18. Computed explicitly, the HS is

$$H_{\hat{G}_2}(\mathbf{z}, t) = \sum_{k=0}^{\infty} \chi_{[0,k]}^{G_2}(\mathbf{z}) t^{2k}, \quad (5.25)$$

displaying a G_2 global symmetry. The Coulomb branch is

$$H_{\hat{G}_2}(t) = H(\overline{min}_{G_2}) \quad (5.26)$$

5.2.5 Comments

From the examples computed, the affine quivers, ungauged at the newly added (or ‘next to minimally imbalanced’) node, displayed a global symmetry of groups of their respective Dynkin diagrams. The Coulomb branch of the moduli spaces were *varieties* called closures of minimal nilpotent orbits (of the same groups). This agrees with the claims made by Hanany & Kalveks [8].

5.3 Ungauging Location

Noting that the short-node ungauged C_n led to a \mathbb{Z}_2 action, we now explore the consequence of changing the ungauging location on the Coulomb branch.

5.3.1 A_n, \hat{A}_n

For A_n , given any ungauged location $1 < j < n$, the HS can be decomposed into a product of HS of A_{j-1} and A_{n-j} , since the two sides are decoupled. This is shown in Fig. 19. The HS is then $H(\mathbb{C}^{2(j-1)}) \times H(\mathbb{C}^{2(n-j)}) = H(\mathbb{C}^{2(n-1)})$; invariant under change of ungauging location.

As for \hat{A}_n , changing the ungauging location does not change the structure of the quiver; therefore its HS is invariant under change of ungauging location.

Regarding topological fugacities, they can always be mapped into the desired basis; therefore they are unimportant in the discussion of Coulomb branch of the moduli space.

$$\begin{aligned}
 & H(\textcircled{1} - \textcircled{1} \cdots \textcircled{1} - \textcircled{1} - \textcircled{1} \cdots \textcircled{1}) \\
 &= H(\textcircled{1} - \textcircled{1} \cdots \textcircled{1} - \textcircled{1}) \\
 &\times H(\textcircled{1} \cdots \textcircled{1} - \textcircled{1})
 \end{aligned}$$

Figure 19: The HS of A_n ungauged at j^{th} node can be decomposed into a product of two smaller A_{j-1} and A_{n-j} quivers.

5.3.2 C_n

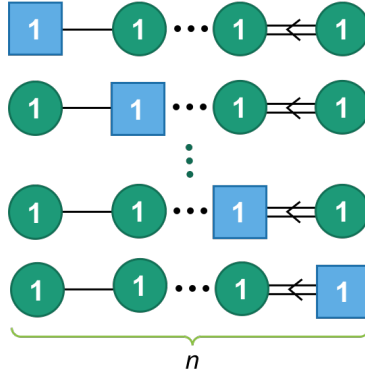


Figure 20: The different cases of ungauging a C_n quiver

Changing the ungauging location for C_n , shown in Fig. 20, apart from the first case and last two cases, the quiver can again be decomposed into a product of A_{j-1} and C_{n-j} for ungauging location $1 < j < n - 1$; so

$$H_{C_n^{(j)}}(t) = H(\mathbb{C}^{2(j-1)}) \times \left(\frac{\mathbb{C}^{2(n-j)}}{\mathbb{Z}_2} \right) = H \left(\mathbb{C}^{2(j-1)} \times \frac{\mathbb{C}^{2(n-j)}}{\mathbb{Z}_2} \right). \quad (5.27)$$

For the second last case, it was analytically (by decomposition) shown that

$$H_{C_n^{(n-1)}}(t) = H(\mathbb{C}^{2(n-2)}) \times H(\mathbb{C}^2/\mathbb{Z}_2) = H(\mathbb{C}^{2(n-2)} \times \mathbb{C}^2/\mathbb{Z}_2), \quad (5.28)$$

which agrees with Eq. (5.27).

The last case has the same HS as A_n , so

$$H_{C_n^{(n)}}(t) = H(\mathbb{C}^{2(n-1)}). \quad (5.29)$$

which also happens to agree with Eq. (5.27). We can see that for a C_n quiver, there is a \mathbb{Z}_2 action on that moves by \mathbb{C}^2 as the ungauged node moves. Also, there is no action on the last (long) node.

5.3.3 F_4, G_2

For the F_4 quiver, the HS's were calculated explicitly, apart from one of the nodes:

$$H_{F_4,a)}(t) = H(\mathbb{C}^{14}) \quad (5.30)$$

$$H_{F_4,b)}(t) = H(\mathbb{C}^{14}) \quad (5.31)$$

$$H_{F_4,c)}(t) : \text{no results yet} \quad (5.32)$$

$$H_{F_4,d)}(t) = H(\mathbb{C}^{10} \times \mathbb{C}^4/\mathbb{Z}_2) \quad (5.33)$$

where $a), b), c), d)$ are as Fig. 21. For long ungauged nodes, we see a flat space of \mathbb{C}^{14} , and for the short node, with \mathbb{Z}_2 action.

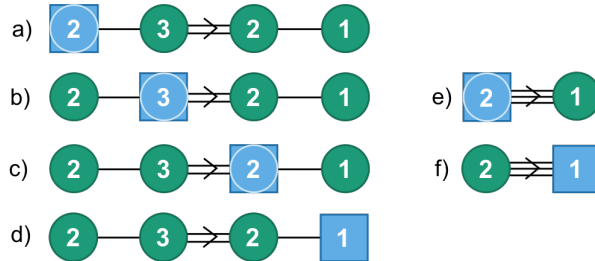


Figure 21: a) ~ d): different ungauging schemes for F_4 quiver; e) ~ f): ungauging schemes for G_2 quiver. Case c) was unable to be calculated due to a technicality with the code.

For G_2 , we see a similar pattern, except the action is \mathbb{Z}_3 , which corresponds to the triply weighted edge of G_2 .

$$H_{G_2,e)}(t) = H(\mathbb{C}^4) \quad (5.34)$$

$$H_{G_2,f)}(t) = H(\mathbb{C}^2 \times \mathbb{C}^2/\mathbb{Z}_3) \quad (5.35)$$

where $e), f)$ are as Fig. 21.

5.3.4 \hat{F}_4, \hat{G}_2

The Coulomb branch of \hat{F}_4, \hat{G}_2 are much more complex. We consult the result of Brylinski & Kostant to deduce that the Coulomb branch of the short nodes are \mathbb{Z}_n action on some parts of the varieties [1].

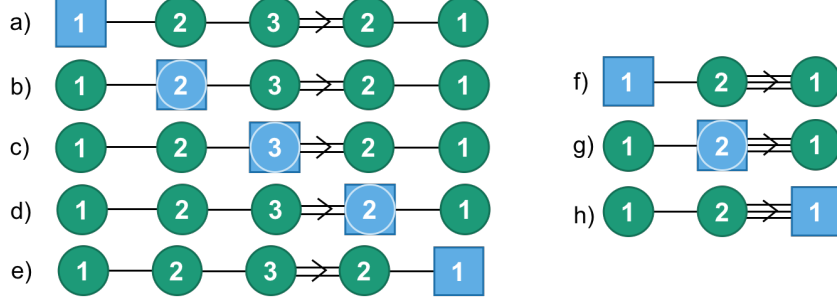


Figure 22: a) \sim e): different ungauging schemes for F_4 quiver; f) \sim h): ungauging schemes for G_2 quiver. Case d) was unable to be calculated due to a technicality with the code.

As Fig. 22, the results are:

$$H_{\hat{F}_4, a, b, c}(t) = H(\overline{\min}_{F_4}) \quad (5.36)$$

$$H_{\hat{F}_4, d}(t) : \text{no results yet} \quad (5.37)$$

$$H_{\hat{F}_4, e}(t) = H(\overline{n.\min}_{B_4}) = H(\overline{\min}_{F_4}/\mathbb{Z}_2) \quad (5.38)$$

where $\overline{n.\min}_{B_4}$ refers to *closure of the next to minimal nilpotent orbits of B_4* , which corresponds to a \mathbb{Z}_2 action on some parts of $\overline{\min}_{F_4}$.

$$H_{\hat{G}_2, f, g}(t) = H(\overline{\min}_{G_2}) \quad (5.39)$$

$$H_{\hat{G}_2, h}(t) = H(\overline{\max}_{A_2}) = H(\overline{\min}_{G_2}/\mathbb{Z}_3) \quad (5.40)$$

where $\overline{\max}_{A_2}$ refers to the *closure of maximal nilpotent orbit of A_2* , which corresponds to $\overline{\min}_{G_2}$.

5.3.5 Comments

From the examples, we see a clear pattern. We state the *Ungauging Hypothesis*: for long nodes and simply laced quivers, the ungauging location does not affect the space of the HS. For short nodes, moving the ungauged node shifts the \mathbb{Z}_n action on some parts of the space where n is the weight of the edges.

6 Conclusion and Outlook

The aim of the project was to study the Coulomb branch of moduli spaces of $\mathcal{N} = 4, d = 2 + 1$ gauge theories, which can be encoded in pictures called quiver diagrams. Moduli space are of interest as they describe the abstract space of vacua. Along the way, intuitions

of representation theory, Hilbert series, and understanding of the monopole formula were developed.

Using a combination of analytic and computational methods, it was found that minimally imbalanced A_n, C_n, F_4, G_2 Dynkin quivers, ungauged at a minimally imbalanced node, displayed symplectic (Sp) global symmetries, and had Coulomb branch of flat spaces \mathbb{C}^n with action of \mathbb{Z}_2 in the case of C_n .

Affine Dynkin quivers, which attaches an additional node to the minimally imbalanced nodes to make the quiver balanced, were ungauged at the newly added node. It was found that they display global symmetries of Lie groups of the same Dynkin names, and that their Coulomb branches are varieties called closures of minimal nilpotent orbits of the same Lie groups. This agrees with the claims made by Hanany and Kalveks [8]. Although due to the complexity of the monopole formula, the Hilbert series were calculated computationally, the global symmetries for \hat{A}_n, \hat{C}_n were shown analytically by counting cases.

Additionally, we explored the implications of changing the location of ungauged node. Arguments in the cases of A_n, \hat{A}_n, C_n , and explicit calculations for $F_4, G_2, \hat{F}_4, \hat{G}_2$, led to the Ungauging Hypothesis: ungauging location for long nodes or simply laced quivers should not have an effect on the Coulomb branch of the moduli space, while changing the ungauging location for short nodes should have a shifting action of \mathbb{Z}_n on the Coulomb branch where n corresponded to the weight of the weighted-directed edge.

However, the Hilbert series for one short node ungauging location for F_4, \hat{F}_4 was not able to be resolved due to complications with the code. Furthermore, there are other Dynkin quivers $B_n, D_n, E_{6,7,8}$ and their affine counterparts to be explored. To further test the hypothesis, the Hilbert series for these examples should be calculated as well. Other directions of further research could be into developing the ‘counting cases’ method to determine global symmetries, perhaps by including the topological fugacities into the calculation.

References

- [1] Brylinski, R., & Kostant, B. (1994). Nilpotent orbits, normality, and Hamiltonian group actions. *Journal of the American Mathematical Society*, 7(2), 269-298.
- [2] M. J. Strassler. An Unorthodox introduction to supersymmetric gauge theory. arXiv:hep-th/0309149
- [3] S. Cremonesi, A. Hanany, A. Zaffaroni. Monopole operators and Hilbert series of Coulomb branches of 3d $N = 4$ gauge theories. arXiv:1309.2657v3 [hep-th]
- [4] D. Gaiotto, E. Witten. S-Duality of Boundary Conditions In $N=4$ Super Yang-Mills Theory. arXiv:0807.3720 [hep-th]
- [5] Sergio Benvenuti, Bo Feng, Amihay Hanany, and Yang-Hui He. Counting BPS Operators in Gauge Theories: Quivers, Syzygies and Plethystics. *JHEP*, 0711:050, 2007.

- [6] Stefano Cremonesi, Giulia Ferlito, Amihay Hanany, Alberto Zaffaroni, Coulomb Branch and The Moduli Space of Instantons, arXiv:1408.6835v2 [hep-th], (2014).
- [7] Stefano Cremonesi, 3d supersymmetric gauge theories and Hilbert series, arXiv:1701.00641v2 [hep-th], (2017).
- [8] Hanany, A., & Kalveks, R. (2016). Quiver theories for moduli spaces of classical group nilpotent orbits. *Journal of High Energy Physics*, 2016(6), 130.
- [9] V. Borokhov, A. Kapustin, X. Wu. Monopole operators and mirror symmetry in three-dimensions. *JHEP*, 0212:044, 2002.
- [10] G. Ferlito. Mirror Symmetry in 3d supersymmetric gauge theories. <https://workspace.imperial.ac.uk/theoreticalphysics/Public/MSc/Dissertations/2013/Giulia>
- [11] D. Bashkirov. Examples of global symmetry enhancement by monopole operators. arXiv:1009.3477 [hep-th].
- [12] Haber, Howie. "SUPERSYMMETRY, PART I (THEORY)" (PDF). Reviews, Tables and Plots. Particle Data Group (PDG). Retrieved 8 July 2015.